Phosphine reactivity and its implications for pyrolysis experiments and astrochemistry

Leonardo Baptista[1*] and Amaury A. de Almeida[2]

[1]Universidade do Estado do Rio de Janeiro, Faculdade de Tecnologia, Departamento de Química e Ambiental, Campus Regional de Resende, Rodovia Presidente Dutra km 298, Rio de Janeiro, RJ - CEP 27537-000, Brazil

[2]Universidade de São Paulo, Instituto de Astronomia, Geofísica e Ciências Atmosféricas, Departamento de Astronomia, Cidade Universitária, Rua do Matão 1226, São Paulo, SP - CEP 05508-090, Brazil

*leobap@gmail.com

Abstract

Despite the importance of phosphorus-bearing molecules for life and their abundance outside Earth, the chemistry of those compounds still is poorly described. The present study investigated phosphine (PH_3) decomposition and formation pathways. The reactions studied include phosphine thermal dissociation, conversion into PO, PN, and reactions in the presence of H_2O^+. The thermodynamic and rate coefficients of all reactions were calculated in the range of 50 – 2000 K considering the CCSD(T)/6-311G(3df,3pd)//ωB97xD/6-311G(3df,3pd) electronic structure data. The rate coefficients were calculated by RRKM and SCTST theories. According to the results, PH_3 is stable due to thermal decomposition at T < 100 K but can be formed promptly by a reaction mechanism involving PH, PO, and PN. In the presence of radiation or ions, PH_3 is readily decomposed. For this reason, it should be mainly associated with dust grains or icy mantles to be observed. The intersystem crossing associated with the dissociation of the isomers PON, NPO, and PNO was accessed by multireference methods, and its importance for the gas-phase PH_3 formation/destruction was discussed. Also, the impact of the present outcomes on the phosphorus space chemistry was highlighted.

Introduction

Phosphorus is a relatively rich cosmical element with [P]/[H]= 3X10-7[1] and an important element in all known life forms. Different phosphorus-bearing compounds have been observed in space[2]. Because phosphorus is a biogenic element, studying the various forms in which it is present in different astronomical environments is a matter of great interest, although still poorly understood[3, 4].

The first phosphorus species found in the molecular clouds was the P=N molecule[5]. The second phosphorus compound detected in interstellar space was the C=P radical[6], found in the circumstellar region around IRC+10216, a late-type evolved star[7]. High-quality ultraviolet observations have confirmed that phosphorus is depleted by approximately a factor of 3 relative to its Solar System abundance in lines of sight containing warm, diffuse clouds and denser cold clouds[8, 9]. Therefore, a significant fraction of interstellar phosphorus must be

trapped in the grain phase. The phosphorus detection as part of the dust components in comet Halley corroborates the previous hypothesis[10].

An emission feature attributed to the J= 1-0 line of PH_3 was observed independently in the spectra of carbon-rich asymptotic giant branch star IRC+10216 and in the envelope of the carbon-rich post-AGB object CRL 2688 from observations of an emission line at 266.9 GHz[11]. Agúndez et al.[12] unambiguously reported the detection of the J= 2-1 rotational transition of PH_3 in IRC+10216, but there is no evidence of its presence in star-forming regions[13]. Two rotational transitions of the PO molecule were observed toward the oxygen-rich red supergiant VY CMa: the J= 5.5 - 4.5 at 239.9 – 240.2 GHz and the J= 6.5 – 5.5 at 283.6 – 283.8 GHz[14, 15].

Recently, Lefloch et al.[16] reported the first detection of PO in solar-type star-forming regions, and Rivilla et al. [17, 18] have shown that P-bearing molecules (in particular, PO and PN) are present in star-forming regions and a quiescent cloud in the Galactic Center. Although their formation process remains poorly understood, PO is a factor 2-3 more abundant than PN. The formation of phosphorus monoxide (PO) from the radiative association of phosphorus and oxygen atoms has been estimated by accurate quantum chemistry calculations by Andreazza et al.[19], and the radiative association between P and S atoms to produce phosphorus monosulfide (PS), also in its doublet ground state, has been investigated by de Almeida et al.[20]. The radiative association of P and Cl atoms to produce phosphorus monochloride (PCl) in its triplet ground state has been investigated by Andreazza et al. [21]. The rate coefficients for forming carbon monophosphide (CP) and silicon monophosphide (SiP) by radiative association were also estimated for temperatures ranging from 300 to 14 100 K by Andreazza et al.[22]. In both cases, rate coefficients increase slowly with the increase in temperature.

Phosphine ice, the phosphorus analog to ammonia (NH_3), is a plausible major phosphorus constituent of comets. However, recent searches in the gaseous coma of a few comets turned out unsuccessful, providing upper limits not significant enough to conclude whether PH_3 locks most of the phosphorus in these small bodies[23, 24]. Phosphorus is in the same chemical family as nitrogen, with an abundance 300 times smaller ([P]/[N]= $4X10^{-3}$). Since P is an essential element in the biochemistry of all living organisms, the detection and abundance determination of P-bearing molecules in comets is of great interest. ROSINA´s double-focusing mass spectrometer (DFMS) of the Rosetta Mission detected atomic P in the coma of Comet 67P/Churyumov-Gerasimenko[25, 26]. It is unclear which parent molecule produces the P seen in the DFMS spectra, taking into account that the instrument measured only the volatile content for O (oxygen) and P. Recently, Rivilla et al.[4] have shown that PO, not atomic phosphorus, is the phosphorus reservoir in Comet 67P/C-G. One would expect simple molecules, such as diatomic species (PH, PO, CP, PN, SiP, P_2, and PCl), triatomic (HCP, CCP and PH_2), and others (PH_3 and diphosphine - P_2H_2), to exist in cometary ices, released into the gas phase upon sublimation.

Despite the molecules' simplicity, phosphorus compounds' chemistry continues to be unknown to those interested in the astrochemistry and astrobiology fields. Until now, few theoretical studies described the PO and PN reactions in ISM conditions[27–32]. While the PH_3 decomposition paths were investigated at higher temperatures to elucidate the epitaxy and

vapor deposition mechanism[33–35]. In parallel, Semenov et al.[36] studied the PN rovibronic spectra theoretically by *ab initio* methods, which is pivotal to helping the correct identification of this molecule by experimental means. Due to these reasons, the present study aims to investigate the pathways for the formation and decomposition of PH_3 and the reactions that may form PO and PN beyond Earth by quantum chemistry methods.

Computational details

The reactions studied are listed in Figure 1 and include phosphine conversion into PO, PN, and reactions in the presence of H_2O^+. The H_2O^+ ion was unambiguously identified in several comets [37–40] and may be a PH_3 sink[41]. All species participating in the reactions were fully optimized and characterized by their harmonic vibrational frequencies. The species considered minima in the potential energy surface (PES) presented only positive frequencies. In contrast, the saddle points that characterize the transition structures of each reaction presented only one imaginary frequency. When appropriate, the anharmonic corrections were calculated by the vibrational second-order perturbation theory (VPT2)[42, 43]. The ωB97xD/6-311G(3df,3pd) level of theory was employed for geometry optimization and frequency calculations.

Further, single-point calculations were performed at CCSD(T)/6-311G(3df,3pd) level. This level of theory was applied successfully in a previous study involving P-bearing molecules of astrochemistry interest[27]. The thermochemical parameters were calculated by the standard equations of statistical thermodynamics. Some reactions investigated involves the participation of excited states and intersystem crossing between potential energy surfaces (PES) with different spin states. The dissociation paths with intersystem crossing were investigated at MRCI (8,8)/cc-pVTZ level, considering the geometries optimized with the DFT method. Due to the nature of the studied species, the wavefunction stability was evaluated to guarantee the proper spin state assignment. All electronic structure calculations were conducted at Gaussian 16[44] and Orca 5.0.1[45].

The kinetic calculations followed different approaches. When appropriate, Miller and collaborators' semiclassical Transition State Theory (SCTST) [46–50] was used for reactions with saddle points. In contrast, the variational version of the RRKM theory was applied for barrierless reactions. The SCTST method was employed, assuming the non-separability of vibrational and rotational motions, and used the anharmonic corrections calculated by the VPT2 method.

All barrierless reactions treated in the present study are dissociation reactions. First, to employ the RRKM theory, a Morse potential was fitted to dissociation paths. Next, we assumed the conservation of all vibrational modes distinct to the mode associated with the reaction coordinate and the vibrational modes non-present in the products. The vibrational frequencies orthogonal to the reaction path, necessary to the RRKM calculation, were obtained, assuming that they can be expressed by Equation 1.

$$\nu = \nu_i + (\nu_f - \nu_i)(1 - e^{(-\alpha(r - r_e))})^2 \quad (1)$$

where ν Is the frequency of the vibrational mode along the reaction path, ν_i is the frequency of the vibrational mode at the reactant geometry, ν_f is the corresponding frequency of the

vibrational mode considering the dissociation products, r_e is de equilibrium distance and α the curvature of the Morse potential. The external moments of inertia were calculated considering different geometries along the dissociation path. The sum of states was minimized in the dissociation path considering the systems' vibrational energy and angular momentum (E and J resolved microcanonical variational TST). Finally, the canonical rate coefficient was obtained by integrating the k(E, J), considering a Boltzmann thermal distribution. When necessary, a master equation was solved[51–55] to evaluate k(T,p), the rate coefficient at the low-pressure limit (k_0^{SC}), and the system dynamics at low pressure and temperature.

All kinetics calculations were performed with the Multiwell 2021 package, and sctst, thermo, bdens, and ktools codes provided with the base package[56–58].

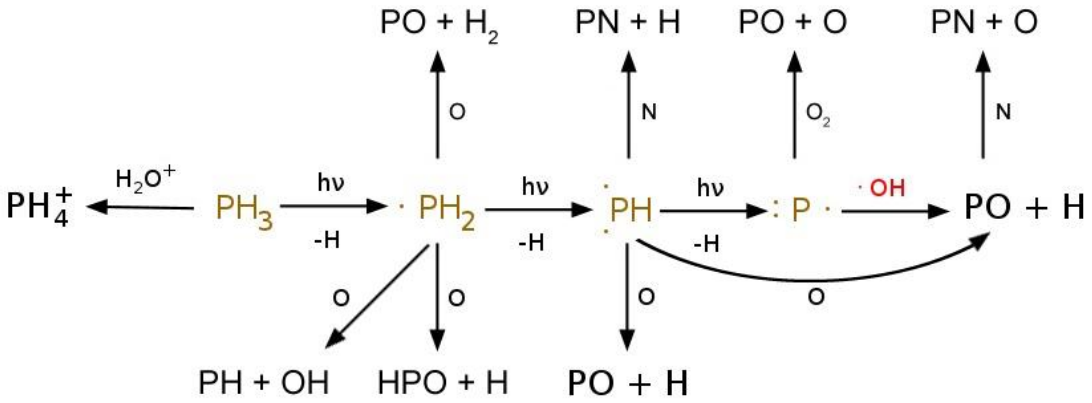

Figure 1: Possible pathways for phosphine decomposition, including the ones considered in the present study.

Results and discussion

First, the thermochemistry of the formation/decomposition of PH_3 and its conversion into PN and PO will be discussed. Next, the kinetic parameters for the reactions studied will be presented, and the reactivity of each specie will be discussed based on the thermodynamic and kinetic parameters. Finally, the implication of the present results for the chemistry of P-bearing molecules in astrochemistry environments will be discussed.

Thermochemistry of the studied systems

Reactions involving PH_3

Figure 2 presents the thermochemistry of the PH_3 reactions in the gas phase. The consecutive phosphine dissociations (right side) and the reactions in the presence of H_2O^+ were studied. As expected, all dissociation channels are highly endothermic, $\Delta_{diss}E$ higher than 75 kcal mol^{-1},

while the reaction with H_2O^+ passes through a pre-barrier complex (RC) that stabilizes the reactants. The high exothermicity for the RC formation indicates a chemically activated adduct formation[59–62].

The RC electronic structure was analyzed by examining the Khon-Shan orbitals, electrostatic potential map, and critical points from the QTAIM methodology[63–65]. This analysis indicates that the structure is a charge transfer complex, where the phosphorus non-ligand electron pairs coordinate to a vacant H_2O^+ orbital (Supplementary material). Further to the RC formation, a hydrogen atom migration occurs, forming an ion-dipole complex (PC) between OH radical and PH_4^+. Finally, PC dissociates into the reaction products.

As ALMA and Rosina teams proposed [9], PH_3 can suffer sequential dissociations in the presence of UV radiation, forming P atoms (Figure 1). Phosphorus atoms can collide with another species, leading to PO or PN molecules previously detected in other systems[4, 26, 30, 31, 66]. Or can condensate, forming solid phosphorus particles, as observed in Jupiter's atmosphere[67]. Our thermochemistry analysis shows that phosphine should be stable in thermal dissociation reactions due to the high energy to break any P-H bond. The same is valid for the subsequent dissociation reactions:

$PH_3 \rightarrow PH_2 + H$ $\Delta_{diss}E_0$ = 79.72 kcal mol^{-1} (77.91 kcal mol^{-1})

$PH_2 \rightarrow PH + H$ $\Delta_{diss}E_0$ = 74.28 kcal mol^{-1} (82.92 kcal mol^{-1})

$PH \rightarrow P + H$ $\Delta_{diss}E_0$ = 68.31 kcal mol^{-1} (66.20 kcal mol^{-1})

The above results were obtained at CCSD(T)/6-311G(3df,3pd)//ωB97xD/6-311G(3df,3pd) and includes ZPE corrections. The values between parenthesis were obtained from the literature, considering reactions occurring in the grains' presence[4, 68, 69]. Our gas-phase outcomes agree with the literature ones, despite the presence or not of a solid specie. The thermochemistry analysis indicates that the recombination reactions, PH_3 formation, are more favorable than the dissociation reactions in the ISM conditions. For this reason, PH_3 should be stable in the absence of radiation fields, ionic species or when protected by the bulk of solid species such as icy mantles[4].

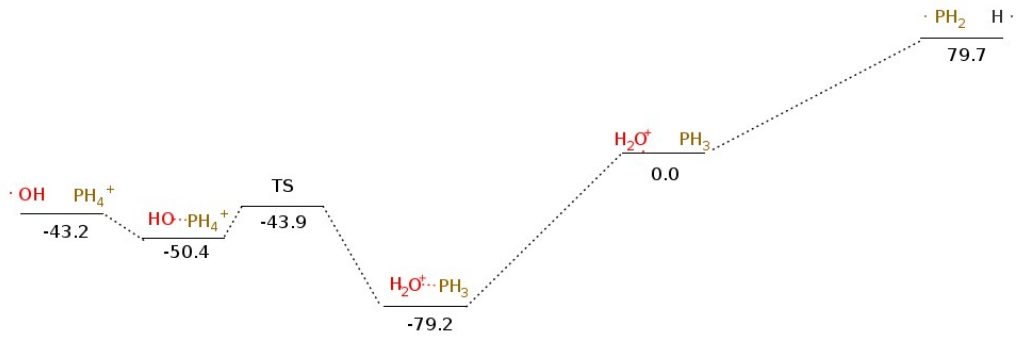

Figure 2: Mechanism for the phosphine decomposition in the presence of H_2O^+ and radiation. Changes in electronic energies corrected by ZPE calculated at CCSD(T)/6-311G(3df,3pd)//ωB97xD/6-311G(3df,3pd). Values in kcal mol^{-1}.

Formation and decomposition of phosphorous monoxide (PO) and phosphorous nitride (PN)

The studied reactions for the PO formation and its conversion in PN are summarized in Figure 3. PO can be formed by collisions between ^{4}P atoms and ^{2}OH radicals, forming the ^{3}P-OH adduct. The adduct has a bent geometry with a θPOH angle of 115.9º, in agreement with the literature[29]. The calculated ΔE_0 value for this reaction is -81.26 kcal mol^{-1}, which is in reasonable agreement with the previous result of -86 kcal mol^{-1}[28]. Since the adduct formation is highly exothermic, it is expected to be chemically activated with the necessary energy to surpass the barrier of 54.15 kcal mol^{-1} forming PO and H atoms. The calculated $\Delta E^{\#}_0$ value is in good agreement with the previous theoretical outcome of 54.33 kcal mol^{-1}[28], which applied a more robust protocol. The present study focuses on the ground state PES, while reactions involving excited electronic states were investigated by de la Concepción and collaborators[28].

Collisions between PH and O atoms can also form phosphorous monoxide. The reaction mechanism proceeds by the formation of OPH in the singlet state, which isomerizes in the electronically excited ^{1}POH molecule. After spin-inversion, ^{1}POH converts into ^{3}POH specie that will undergo the previously discussed reactions.

After the PO formation, this molecule can collide with N atoms to produce PN. However, the N atom can interact directly with the P atom, forming the linear specie ^{1}NPO, or bind to the oxygen atom, forming the linear stable specie ^{1}PON. PON has bent excited states with quintet multiplicity. The ^{5}PON formation has a saddle point in the reaction path, while the ^{1}PON and ^{1}NPO formation are barrierless and highly exothermic. The spectroscopic properties of ^{1}PON and ^{1}NPO were investigated previously by Zeng et al.[70] and the electronic structure of PON isomers and its ions by Grant and collaborators[71]. According to Zeng, NPO can be selectively converted to PNO by photolysis using radiation with $\lambda > 320$ nm[70].

The ^{1}PON dissociation into ^{2}PO + ^{4}N has three intersystem crossing (figure 4a). As the rON bond distance is stretched, different electronic states becomes more stable. At 1.9 Å, the triplet surface becomes the more stable state, while at distances higher than 4.9 Å, the quintet state becomes the more stable. The existence of three intersystem crossings shows the complexity behind the electronic structure of this molecule and indicates that single-reference methods may fail to describe the dynamics of this system.

^{1}PON can isomerize into ^{1}NPO via a bent transition structure with a critical energy of nearly 51 kcal mol^{-1}. According to Souza et al.[29], the NPO has a bent triplet ground state, with a θNPO of 120º and a second bent geometry, with θNPO = 107º, with approximate energy. However, at the DFT level, we cannot optimize the geometry with θNPO = 107º, and at CCSD(T)/6-311G(3df,3pd)//ωB97xD/6-311G(3df,3pd) level, the linear singlet is 32 kcal mol^{-1} most stable than the triplet state. Was also obtained an angular singlet, with θNPO = 64.78º and 33 kcal mol^{-1} above the linear singlet.

Another possible isomerization is the ^{1}NPO conversion into ^{1}PNO with linear geometry. Further, ^{1}PNO can dissociate into ^{1}PN and ^{3}O. However, the products' ground state formation occurs through an intersystem crossing between the singlet and triplet states (Figure 4b).

Also, the formation of ^{1}NPO occurs via an intersystem crossing between the triplet surface, which describes the ^{2}PO and ^{4}N ground state, with the singlet surface. This crossing can be observed in Figure 4c, which shows the N-P bond changing at MRCI(8,8)/cc-pVTZ//wB97Xd/6-311G(3df,3dp) level. Nearly to 2.1 Å, the singlet surfaces cross the triplet surface, and at longer bond distances, the triplet state becomes the system's ground state.

Figure 4d shows that the reaction path for ^{1}NPO dissociation in ^{1}PN and ^{3}O also has an intersystem crossing between the singlet and triplet surfaces. The crossing occurs at 2.0 Å, and the triplet becomes the ground state at longer bond distances. The dissociation energy for this reaction is $\Delta_{diss}E_0$ = 79.67 kcal mol^{-1}. It is also expected the formation of chemically activated ^{1}NPO specie due to the reaction exothermicity. Consequently, the formation of ^{1}PN and ^{3}O species in the reaction should be expected[51, 55, 62, 72].

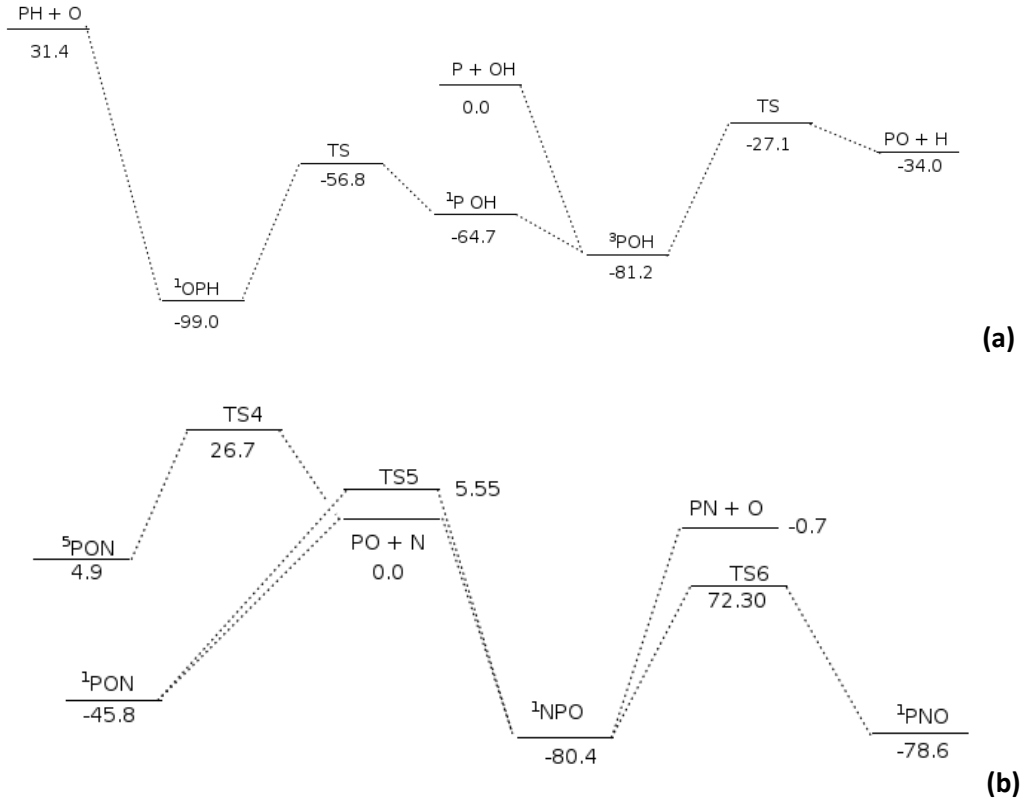

Figure 3: a) Reaction mechanism for the formation of PO from P + OH reaction and interconversion of PO into PH. b) Interconversion mechanism of PO into PN. Changes in electronic energies corrected by ZPE calculated at CCSD(T)/6-311G(3df,3pd)// ωB97xD/6-311G(3df,3pd). Values in kcal mol^{-1}.

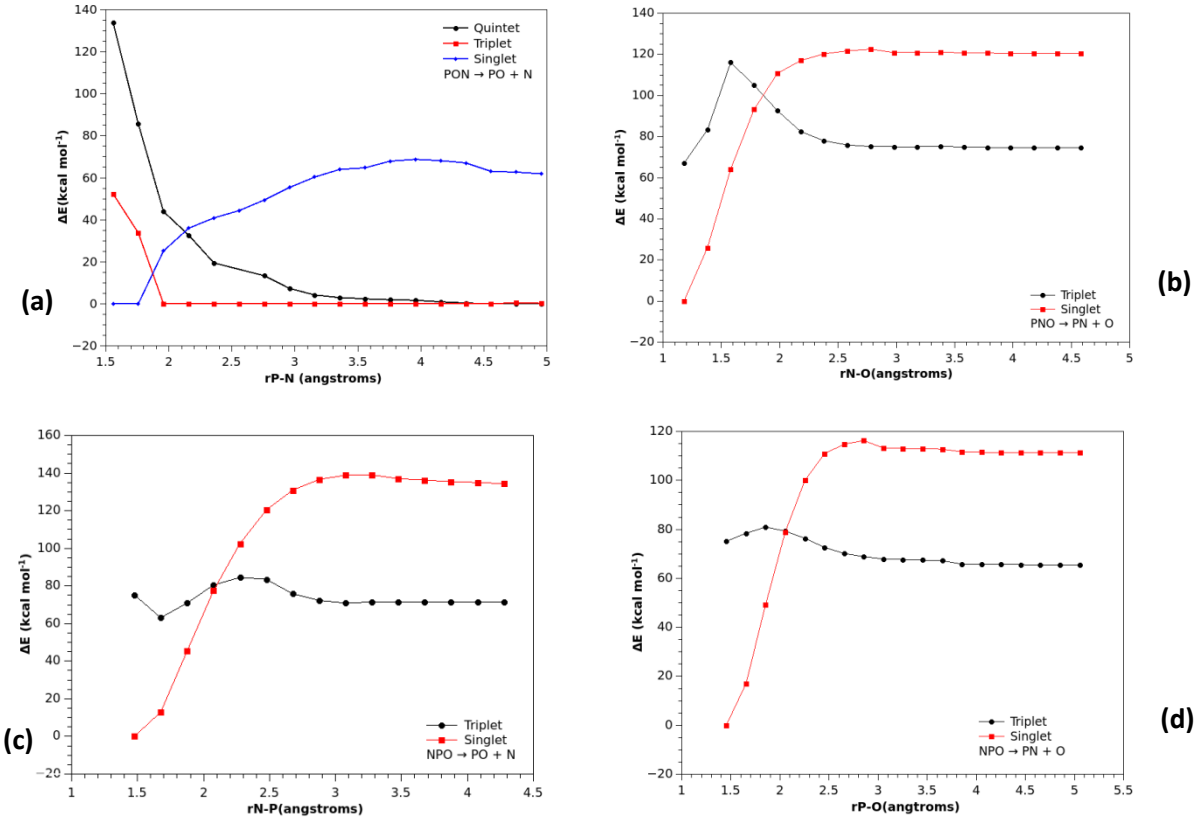

Figure 4: Intersystem crossing observed for the NPO, PNO, and PON dissociations. Changes in electronic energy calculated at MRCI(8,8)/cc-pVTZ)// ωB97xD/6-311G(3df,3pd). Values in kcal mol^{-1}. a)^{1}PON dissociation into ^{2}PO + ^{4}N. b)^{1}PNO dissociation into ^{3}O + ^{1}PN. c)^{1}NPO dissociation into ^{2}PO + ^{4}N. d)^{1}PON dissociation into ^{1}PN + ^{3}O.

Kinetics of the studied systems

Rate coefficients for the PH_3 consecutive dissociations

During pyrolysis or in the ISM, consecutive PH_3 dissociations are expected by homolytic fission of the P-H bond[4, 33, 34]. The unimolecular processes should compete with other bimolecular reactions of PH_3[4, 28, 73, 74]. However, the dissociation must be analyzed to infer their role in forming P-bearing molecules in the ISM. The three dissociation/recombination reactions studied are listed in Figure 1.

The Arrhenius parameters fitted to the calculated rate coefficients at the high-pressure limit are listed in Table 1, showing the temperature range where the parameters are valid. The equilibrium constant equation fitted in all ranges of temperatures studied is available in the Supplementary material to those interested in obtaining the dissociation or recombination rate coefficient at different temperatures.

The Arrhenius parameters for the dissociation reactions were fitted only for temperatures above 1000 K because thermal dissociation is important only at high temperatures, as

reported previously[33, 34]. The calculated high-pressure rate coefficients for the $PH_3 \rightarrow PH_2 + H$ reaction agrees with Buchan results[33] at high temperature, but the outcomes deviates as the temperature lowers (Figure 3). The k_∞ results of Cardelino et al.[75] are overestimated in comparison with the present and Buchan results. Mulvihill et al.[34] studied the same reactions by shock tube experiments at Ar bath, at 0.5 and 1.3 atm. He stated that the measured rate coefficient is at the low-pressure limit and can be expressed as

$$k_0(T) = [Ar]29 \times 10^{-6}(cm^3 molec^{-1} s^{-1})\exp(-\frac{80400(cal\ mol^{-1})}{RT}) \text{ [34]} \quad (2)$$

The input data and the outcomes of the RRKM calculation using the ktools code were used to solve a master equation and calculated the low-pressure limit rate coefficient assuming the strong collision hypothesis, $k_0^{SC}(T)$. The fitted Arrhenius equation is:

$$k_0^{SC}(T) = [Ar]5.2 \times 10^{16}(cm^3 molec^{-1} s^{-1})\mathrm{T}^{-6.2}\exp(-\frac{23424(cal\ mol^{-1})}{RT}) \quad (3)$$

The comparison between equations 3 and 4 is depicted in Figure 5. The present results are higher than the experimental measurements[34] and should be related to the strong collision assumptions, which reduces the dissociation activation energy. As performed in the literature[76], the weak collision efficiency β_c, was estimated as $\beta_c = \frac{k_0\ (T)}{k_0^{SC}(T)}$ for the PH_3 dissociation in Ar bath. β_c was evaluated in the range of 1400-2000 K, since the coefficients measured by Mulvihill are strictly valid at this range. The β_c values span from 1.071 to 1.081 in this range of temperatures.

Master equation simulations were also conducted to investigate the rate coefficient dependency with pressure and the photodissociation in the presence of the typical radiation fields[4]. The fall-off curves for the dissociation reactions are presented in the Supplementary Material, in the range of 1000 K to 2000 K. They were calculated by multiplying the fraction of reactants at the end of the simulation ($f(t_{max})$) by the recombination rate coefficient at the high-pressure limit. Next, the dissociation rate coefficient, $k_{uni}(T,p)$, was calculated by the relationship between rate coefficients and the equilibrium constant

$$k_{rec} = k_{rec}^{\infty}(T) f(t_{max})$$

$$K_{eq} = \frac{k_{uni}}{k_{rec}}$$

The $k_{uni}(T,p)$ graphs show that the high-pressure limit is reached above 300 atm, corroborating Mulvihill and collaborators' statement that the measurements at 0.5 atm can be considered at the low-pressure limit[34].

To evaluate the photodissociation rate, we considered that the radiation of 6-13 eV, far UV, increases the vibrational temperature of the thermal population by the photon energy. All master equation simulations conducted at low pressure, 0.01 atm, and 10 K resulted in readily complete phosphine dissociation. Despite the high PH_3 stability relative to thermal decomposition, the photodissociation process can be an effective PH_3 sink.

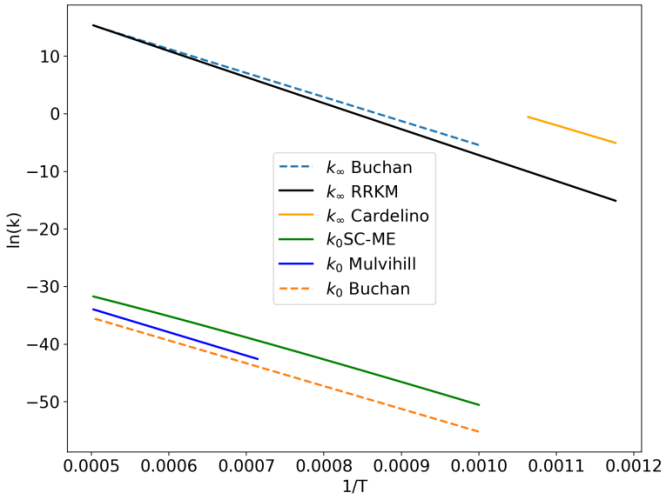

Figure 5: Rate coefficients at the high-pressure limit(k_∞) and low-pressure limit (k_0) for the $PH_3 \rightarrow H + PH_2$ dissociation. k_∞ RRKM refers to the rate coefficients calculated by RRKM theory, and k_0SC-ME refers to the low-pressure limit rate coefficient calculated by solving a master equation assuming the strong collision model.

Without radiation or reactive species, such as free radicals or ions, at low pressure and low temperature, PH_3 will not undergo decomposition reactions. At the same time, recombination reactions of PH_x (x = 0-2) with H atoms will lead to PH_3 formation and accumulation. The analysis of the equilibrium constants shows that the dissociation reaction surpasses the recombination reaction at 900 K, being dominant at temperatures higher than 1000K. Identifying astrochemical processes leading to the synthesis, stability, and decomposition of phosphine by subsequent H additions or in the presence of H_2 at ambient conditions is relatively tricky due to the gas phase's low pressure and H concentration [4, 69]. However, the present outcomes show that PH_3 is a stable specie readily formed by collisions between P and H atoms, in the presence or not of solid species.

Rate parameters for the $PH_3 + H_2O^+$ reaction

The rate coefficients at the high-pressure limit for the $PH_3 + H_2O^+$ reactions were evaluated by the E and J resolved RRKM theory, followed by integration at 50-1000K. The rate coefficients for the RC formation were obtained after a Morse potential fit to the RC dissociation path into reactants. The vibrational frequencies along the reaction path were calculated by Equation 1 if the RC frequencies should converge to the separated reactants' vibrational frequencies and rotational constants. The moments of inertia were evaluated at each point of the dissociation path and used in conjunction with the vibrational frequencies for the RRKM variational calculations. Further, the rate coefficients for the RC formation were evaluated by the relationship between the equilibrium constant and the direct and reverse rate coefficients.

Table 1: Arrhenius's parameters calculated for the studied reactions. It is given the range of temperatures where each fit is valid.

$k_\infty(T)$	ln(A)	m	Ea/R	T(K)
$PH_3 \rightarrow PH_2 + H$	31.34	0.81	44141.77	1000-2000
$PH_2 + H \rightarrow PH_3$	-24.47	0.44	-77.39	100-1000
$PH_2 \rightarrow PH + H$	36.40	0.20	40982.2	1000-2000
$PH + H \rightarrow PH_2$	-23.24	0.67	120.36	100-1000
$PH \rightarrow P + H$	25.30	0.12	36940.07	1000-2000
$P + H \rightarrow PH$	-27.05	-0.13	459.99	50-1000
$P + OH \rightarrow POH$	-21.61	0.16	128.41	100-1000
$POH \rightarrow P + OH$	40.01	-0.61	43106.66	1000-2000
$POH \rightarrow PO + H$	21.43	1.279	26690.87	50-2000
$PO + N \rightarrow {}^5PON$	-117.76	12.94	5289.19	50-2000
${}^5PON \rightarrow PO + N$	-60.04	12.04	7255.33	50-2000
${}^1NPO \rightarrow {}^1PON$	25.99	2.10	42941.17	100-2000
${}^1PON \rightarrow {}^1NPO$	25.15	1.09	26392.05	100-2000
${}^1NPO \rightarrow {}^1PNO$	11.51	1.60	37114.24	100-2000
${}^1PNO \rightarrow {}^1NPO$	10.91	1.76	37125.78	100-2000

The fitted Arrhenius parameters to theoretical rate coefficients, calculated by RRKM theory, are:

$$PH_3 + H_2O^+ \rightarrow PC1$$

$$k(T) = 6.3 \times 10^{34}(cm^3 molec^{-1} s^{-1}) T^{6.8} \exp\left(-\frac{671.17(cal\ mol^{-1}}{RT}\right) (100 - 2000K) (4)$$

$$PC1 \rightarrow PH_3 + H_2O^+$$

$$k(T) = 2.4 \times 10^{30}(cm^3 molec^{-1} s^{-1}) T^{-3.5} \exp\left(-\frac{85200.16(cal\ mol^{-1}}{RT}\right) (100 - 2000K) (5)$$

$$PC1 \rightarrow PC2$$

$$k(T) = 1.15 \times 10^{12}(s^{-1}) T^{0.46} \exp\left(-\frac{35384.10(cal\ mol^{-1}}{RT}\right) (100 - 2000K) (6)$$

$$PC2 \rightarrow PC1$$

$$k(T) = 1.15 \times 10^{34}(cm^3 molec^{-1} s^{-1}) T^{0.46} \exp\left(-\frac{28937.59(cal\ mol^{-1}}{RT}\right) (100 - 2000K) (7)$$

RC is a charge transfer complex, for this reason, a deviation from the harmonic oscillator approach should be expected for the modes involving the P-O bond. Also, coupling between the vibrational and rotational modes must be necessary to evaluate rate coefficients for RC reactions. The effect of anharmonicities corrections and the coupling between the vibrational and rotational modes were included in the k(T) calculation by using the semiclassical Transition State Theory (SCTST) of Miller[47, 48, 77–80]. The comparison of the obtained Arrhenius equations is shown in Figure 4. The reaction studied was the reversible $RC \rightleftharpoons PC$ conversion. The results shown that the direct reaction is not influenced by the anharmonic corrections, while the reverse path is sensitive to these corrections. PC is an ion-dipole complex without a covalent bond between the fragments. This weak intermolecular interaction contributes to deviations in the harmonic oscillator, and rigid rotors approaches adopted in the RRKM method.

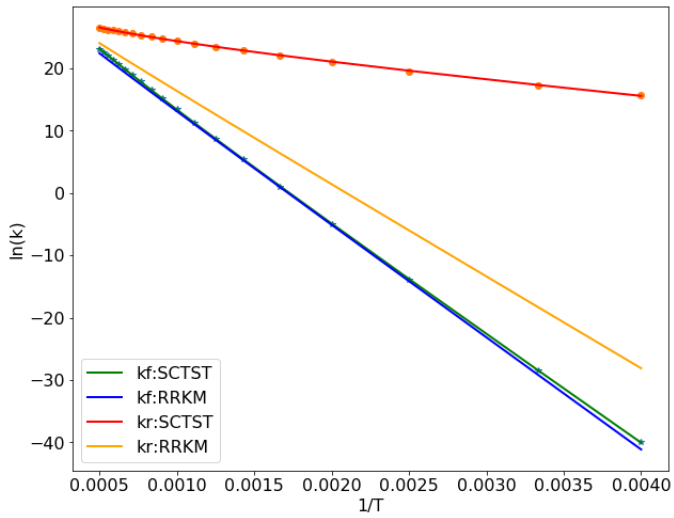

Figure 6: Rate coefficients for the RC ↔ PC interconversion calculated according to different methodologies. The parameters were calculated using the vibrational properties and geometric parameters calculated at ωB97xD/6-311G(3df,3pd) level and barrier heights at CCSD(T)/6-311G(3df,3pd)// ωB97xD/6-311G(3df,3pd) level.

Since the PH_3 + H_2O^+ reaction is not elementary, passing through a reactive pre-barrier complex, which can be chemically activated, a master equation simulation was performed to assess the low-pressure and low-temperature system dynamics. The simulations were conducted at p = 0.001 – 400 atm and T = 100 – 300 K considering the formation of a chemically activated $[H_2O\text{---}PH_3]^+$ complex. Lowers temperatures were not possible to achieve due to the magnitude of reaction barriers that slower the reactions at T < 100, a difficulty in the master equation solution. It was verified that the rate coefficients for the RC dissociation into H_2O^+ plus PH_3 are nearly zero below 100 K. Figure S6 shows the steady-state fraction of each specie at the end of simulations as a function of the initial pressure. At 100 K and pressures below 1 atm, the major species are the RC and the reactants. At high pressure, the RC accounts for more than 90% of the species participating in the mechanism. However, at 200 K and pressures below 100 atm, the system is mainly composed of separated reactants. The PC fraction at lower pressures may be neglected due to its lower value.

The reaction flux analysis shows the rapid formation of the reactants and PC at the beginning of the simulation, Figure S6c. As the reaction evolves, PC converts back into RC, and the RC → reactants flux goes to zero after 0.1 μs at 0.1 atm. According to the results, the formation of PH_4^+ and OH is minor and most significant at pressures below 0.5 atm. At this range of pressures, the reaction products contribute with 1-9% of the species in the system.

If the RC is formed chemically activated at the gas phase and lower pressure, it decomposes back into the reactants. RC is stabilized by collisions and should accumulate in the system at high pressures with high collision rates, such as solid bulks or icy mantles. Additional simulations were conducted considering a thermal distribution of energies for all species. In this case, the RC complex is the only specie at the end of the simulations. This result corroborates the hypothesis that if the adduct is formed, it may accumulate in the absence of radiation or other reactants.

Kinetics of the P + OH reactions

The rate coefficient at the high-pressure limit for the formation of the P-OH adduct was calculated by the variational version of the E and J resolved RRKM theory. At the same time, the coefficient for the O-H bond break was evaluated by SCTST theory. All coefficients were evaluated at a high-pressure limit, and the Arrhenius parameters for both reactions are listed in Table 1.

Despite the PO abundance in the ISM, there is a lack of kinetic data about its formation and reactions. Previously, de la Concepción and collaborators[28] calculated the rate coefficients for PO formation by solving a one-dimensional master equation at 10^{-7} atm and 30-400 K. To our knowledge, there is no other kinetic data about PO reactions. As mentioned early, the entrance channel for PO formation is a barrierless adduct formation. This adduct converts into PO + H, passing by a saddle point. At low temperatures, the adduct may be stable to dissociation reactions; however, due to the reaction exothermicity, it may be formed chemically activated, making possible the PO formation. The equilibrium constant analysis indicates that POH back reaction into reactants is only important at temperatures higher than 800 K. At this temperature, the adduct dissociation reactions become more important than its formation reactions. At higher temperatures, the reverse reaction $PO + H \rightarrow POH$ competes with the reaction $P + OH \rightarrow POH$, pointing that the POH molecule should accumulate in determined conditions.

Kinetics of the PO + N reactions

Since the known statistical rate theory is strictly valid when no intersystem crossing occurs between two different electronic states, the rate coefficients for the PO + N collision was only calculated for the ^{5}PON formation assuming no influence of different electronic states on the quintet PES. The PO ↔ PN interconversion was previously studied in the literature[29] using multireference methods to describe the intersystem crossing between different electronic

states. This result agrees with the present outcomes showing the complexity of the reaction mechanism involving P-bearing species in the interstellar medium. It was also demonstrated that the dissociation reactions of PON isomer involve different electronic states' participation.

For the presented reasons, the ^{5}PON formation was calculated by SCTST theory for the atom-diatom collision (PO + N). The coupling between rovibrational modes and anharmonic corrections on the vibrations was assumed. The Arrhenius' equation for the direct and reverse reaction was fitted in the 50-2000 K range and is shown in Table 1. Also, the rate coefficients for the reactions $^1PON \rightarrow {}^1NPO$ and $^1NPO \rightarrow {}^1PNO$ were calculated via RRKM theory. The results show that no isomerization reaction should be expected at lower temperatures in the gas phase. All interconversions are very slow at temperatures below 100K if the energy excess of PON isomers is removed by collisions[59].

Despite the possibility of PN formation by the channel PON → PNO → PN + O, the barrier heights are impeditive at low temperatures. The most favorable channel is through the formation of NPO with further dissociation in PN + O. Indeed, Smith et al.[81] proposed the following Arrhenius' rate equation based on experiments that some neutral-neutral reaction occurs fast at low temperatures with no activation barrier:

$$k(T) = 3.0 \times 10^{-11} \left(\frac{T}{300}\right)^{-0.60} \quad 10\ K < T < 300\ K \quad (8)$$

Also, Douglas et al. obtained the equation $9.8 \times 10^{-11} \exp(175/T)$ by solving a master equation. The obtained activation energy is -0.35 kcal mol^{-1}, showing negative dependence with the temperature and a small negative barrier, indicating that the reaction is not elementary. The present outcomes corroborate the Arrhenius' equations proposed in the literature for the PO + N → PN + O reaction is not elementary and may rapidly occur via the formation of chemically activated species. All results show that the product's ground state has almost the same energy that the reactants at its ground state. Also, the literature's results indicate that if the PON intermediate is produced, it should decompose prompt into products, indicating that it may be formed chemically activated, as discussed previously in the literature[82, 83].

Implications for astrochemistry

Phosphine (PH_3) ice, the phosphorus analog to ammonia (NH_3), is a super volatile species like CO and CO_2 and a plausible major phosphorus constituent of comets. However, recent searches in the gaseous coma of a few comets turned out unsuccessful, providing upper limits not significant enough to conclude whether or not PH_3 locks most of the phosphorus in these small bodies[23, 24].

As the main constituent of the Jovian atmosphere is molecular hydrogen, essentially all the phosphorus is present in the form of PH_3 [84–86]. In the giant planets, phosphorus is found in the PH_3 form, and the volume mixing ratio is about 10-6 on Jupiter[86, 87]. However, the presence of such element in the deck clouds of Venus is still under debate[74, 88–91]. Though PH_3 is not the most thermodynamically favorable form of gas-phase phosphorus at

temperatures of the Venus atmosphere, PH_3 formed in the hot deep layers should be brought to the top of the atmosphere through convective transport.

At lower temperatures (T < 100 K), phosphine is a stable molecule through thermal decomposition; however, it can be readily decomposed when irradiated by far UV radiation or in the presence of free radicals or ions. The PH_3 reactivity may be associated with the issues of characterizing and quantifying it unambiguously in comets and planetary atmospheres. However, PO and PN may be considered PH_3 decomposition products and may be used as markers for the presence of phosphine in some environments.

Douglas et al.[30] proposed an update in the reaction network involving P-bearing species. The network includes the formation of PH that can form PH_3 by successive H addition. However, reactions involving PH_3 and the PON isomers must be included explicitly in the network. This statement is corroborated by the previous observation of the photo-induced conversion of NPO into PNO and how this process can be important to surpass the high thermal barriers between these isomers[70].

In planetary atmospheres, the PH_3 dissociation reactions will occur at the low-pressure limit, which is a slow process. Consequently, this specie must be stable under atmospheric conditions and degraded only in the presence of free radicals, ions, and radiation. This finding agrees with the PH_3 lifetime estimative of Greaves et al.[73, 74]. According to the authors, the difference between the PH_3 abundance in Venus' and Earth's atmospheres is due to the substantial amount of molecular oxygen and their photochemical radicals.

Conclusions

Phosphine and gaseous P-bearing molecules are certainly of broad interest in astrochemistry environments such as interstellar and circumstellar space, gas giant planets, cometary atmospheres, and potential biosignatures[92].

In the present study, different reactions involving PH_3 decomposition and their reaction intermediates describe the chemistry of P-bearing molecules astrochemistry. Also, the fall-off curves of PH_3 dissociation were calculated at high temperatures to complete the mechanism of epitaxy described in the literature. The results show that PH_3 is stable in low pressure and temperature if high energy radiation and ions are absent.

Despite a large number of P-molecules considered by Seager et al.[93], the constraints imposed when constructing the "CNOPSH List" exclude molecules considered in our work, such as the radicals PO, PN, and PH, which are stable diatomic species and products of PH_3 decomposition. The reaction mechanism of the interconversion of these species by atom-diatomic molecule collision and isomerization proved complex. In some cases, the reaction pathway has an intersystem crossing between different spin states, which difficult the rate coefficients calculation by the conventional statistical rate theories.

The chemistry of the three PON isomers proved complex due to the intersystem crossing observed in their dissociation pathways. However, all isomers are stable and may accumulate

in the appropriate conditions. The reaction rate coefficients should include the surface hopping between different spin states for modeling purposes.

The calculated rate coefficients for the PH_3 decomposition/formation were expressed as a function of the temperature in the high-pressure and low-pressure limits. These kinetic parameters can be included in astrochemistry databases, like UMIST, which does not include phosphine, to be used in future modeling of different space environment conditions.

We conclude that, given the low reactivity of many gas-phase P-bearing molecules and the relatively poor understanding of gaseous phosphorus chemistry, an update in the reaction network involving P-bearing species, particularly phosphine, is necessary.

References

1. Asplund M, Grevesse N, Sauval AJ, Scott P (2009) The chemical composition of the Sun. Annu Rev Astron Astrophys 47:481–522. https://doi.org/10.1146/annurev.astro.46.060407.145222

2. Margulès L, Herbst E, Ahrens V, et al (2002) The Phosphidogen Radical, PH2: Terahertz Spectrum and Detectability in Space. J Mol Spectrosc 211:211–220. https://doi.org/10.1006/JMSP.2001.8500

3. Maciá E (2005) The role of phosphorus in chemical evolution. Chem Soc Rev 34:691–701. https://doi.org/10.1039/B416855K

4. Rivilla VM, Drozdovskaya MN, Altwegg K, et al (2020) ALMA and ROSINA detections of phosphorus-bearing molecules: the interstellar thread between star-forming regions and comets. Mon Not R Astron Soc 492:1180–1198. https://doi.org/10.1093/mnras/stz3336

5. Turner BE, Bally J (1987) Detection of interstellar PN - The first identified phosphorus compound in the interstellar medium. Astrophys J 321:L75. https://doi.org/10.1086/185009

6. Guélin M, Cernicharo J, Paubert G, Turner BE (1990) Free cp in irc+ 10216. Astron Astrophys 230:L9--L11

7. MacKay DDS, Charnley SB (2001) Phosphorus in circumstellar envelopes. Mon Not R Astron Soc 325:545–549. https://doi.org/10.1046/J.1365-8711.2001.04429.X/2/M_325-2-545-EQ038.JPEG

8. York DG (1994) The elemental composition of interstellar dust. Science (80-) 265:191–192. https://doi.org/10.1126/science.265.5169.191

9. Kwok S (2006) Physics And Chemistry of the Interstellar Medium. University Science Books

10. Kissel J, Krueger FR (1987) The organic component in dust from comet Halley as measured by the PUMA mass spectrometer on board Vega 1. Nat 1987 3266115 326:755–760. https://doi.org/10.1038/326755a0

11. Tenenbaum ED, Ziurys LM (2008) A Search for Phosphine in Circumstellar Envelopes:

PH 3 in IRC +10216 and CRL 2688? . Astrophys J 680:L121–L124. https://doi.org/10.1086/589973/FULLTEXT/

12. Agúndez M, Cernicharo J, Decin L, et al (2014) CONFIRMATION OF CIRCUMSTELLAR PHOSPHINE. Astrophys J Lett 790:L27. https://doi.org/10.1088/2041-8205/790/2/L27

13. Jiménez-Serra I, Viti S, Quénard D, Holdship J (2018) The Chemistry of Phosphorus-bearing Molecules under Energetic Phenomena. Astrophys J 862:128. https://doi.org/10.3847/1538-4357/AACDF2

14. Tenenbaum ED, Woolf NJ, Ziurys LM (2007) Identification of Phosphorus Monoxide (X 2 Π r) in VY Canis Majoris: Detection of the First P–O Bond in Space . Astrophys J 666:L29–L32. https://doi.org/10.1086/521361/FULLTEXT/

15. Tenenbaum ED, Dodd JL, Milam SN, et al (2010) THE ARIZONA RADIO OBSERVATORY 1 mm SPECTRAL SURVEY OF IRC +10216 AND VY CANIS MAJORIS (215–285 GHz). Astrophys J Suppl Ser 190:348. https://doi.org/10.1088/0067-0049/190/2/348

16. Lefloch B, Vastel C, Viti S, et al (2016) Phosphorus-bearing molecules in solar-type star-forming regions: first PO detection. Mon Not R Astron Soc 462:3937–3944. https://doi.org/10.1093/MNRAS/STW1918

17. Rivilla VM, Jiménez-Serra I, Zeng S, et al (2018) Phosphorus-bearing molecules in the Galactic Center. Mon Not R Astron Soc Lett 475:L30–L34. https://doi.org/10.1093/MNRASL/SLX208

18. Rivilla VM, Fontani F, Beltrán MT, et al (2016) THE FIRST DETECTIONS OF THE KEY PREBIOTIC MOLECULE PO IN STAR-FORMING REGIONS. Astrophys J 826:161. https://doi.org/10.3847/0004-637X/826/2/161

19. Andreazza CM, de Almeida AA, Borin AC (2016) The radiative association of P and O atoms. Mon Not R Astron Soc 457:3096–3100. https://doi.org/10.1093/MNRAS/STW116

20. de Almeida AA, Andreazza CM, Borin AC (2020) Formation of PS through radiative association. Theor Chem Acc 139:1–6. https://doi.org/10.1007/S00214-020-2545-8/TABLES/1

21. Andreazza CM, de Almeida AA, Costa GJ, Borin AC (2020) Radiative association of P and Cl atoms. Theor Chem Acc 139:1–6. https://doi.org/10.1007/S00214-020-02606-Y/FIGURES/3

22. Andreazza CM, Marinho EP, Singh PD (2006) Radiative association of C and P, and Si and P atoms. Mon Not R Astron Soc 372:1653–1656. https://doi.org/10.1111/J.1365-2966.2006.10964.X/2/M_MNRAS0372-1653-M7.GIF

23. Crovisier J, Bockelée-Morvan D, Colom P, et al (2004) The composition of ices in comet C/1995 O1 (Hale-Bopp) from radio spectroscopy - Further results and upper limits on undetected species. Astron Astrophys 418:1141–1157. https://doi.org/10.1051/0004-6361:20035688

24. Agúndez M, Biver N, Santos-Sanz P, et al (2014) Molecular observations of comets C/2012 S1 (ISON) and C/2013 R1 (Lovejoy): HNC/HCN ratios and upper limits to PH_3. Astron Astrophys 564:L2. https://doi.org/10.1051/0004-6361/201423639

25. Altwegg K, Balsiger H, Bar-Nun A, et al (2016) Prebiotic chemicals-amino acid and phosphorus in the coma of comet 67P/Churyumov-Gerasimenko. Sci Adv 2:. https://doi.org/10.1126/SCIADV.1600285

26. Rubin M, Altwegg K, Balsiger H, et al (2019) Elemental and molecular abundances in comet 67P/Churyumov-Gerasimenko. Mon Not R Astron Soc 489:594–607. https://doi.org/10.1093/mnras/stz2086

27. Viana RB, Pereira PSS, Macedo LGM, Pimentel AS (2009) A quantum chemical study on the formation of phosphorus mononitride. Chem Phys 363:49–58. https://doi.org/10.1016/j.chemphys.2009.07.008

28. García de la Concepción J, Puzzarini C, Barone V, et al (2021) Formation of Phosphorus Monoxide (PO) in the Interstellar Medium: Insights from Quantum-chemical and Kinetic Calculations. Astrophys J 922:169. https://doi.org/10.3847/1538-4357/ac1e94

29. Souza AC, Silva MX, Galvão BRL (2021) Interconversion mechanisms of PN and PO in the interstellar medium through simple atom–diatom collisions. Mon Not R Astron Soc 507:1899–1903. https://doi.org/10.1093/MNRAS/STAB2255

30. Douglas KEVM, Gobrecht D, Plane JMC (2022) Experimental study of the removal of excited state phosphorus atoms by H2O and H2: implications for the formation of PO in stellar winds. Mon Not R Astron Soc 515:99–109. https://doi.org/10.1093/MNRAS/STAC1684

31. Douglas KM, Blitz MA, Mangan TP, Plane JMC (2019) Experimental Study of the Removal of Ground- and Excited-State Phosphorus Atoms by Atmospherically Relevant Species. J Phys Chem A 123:9469–9478. https://doi.org/10.1021/acs.jpca.9b07855

32. Douglas KM, Blitz MA, Mangan TP, et al (2020) Kinetic Study of the Reactions PO + O2and PO2+ O3and Spectroscopy of the PO Radical. J Phys Chem A 124:7911–7926. https://doi.org/10.1021/acs.jpca.0c06106

33. Buchan NI, Jasinski JM (1990) Calculation of unimolecular rate constants for common metalorganic vapor phase epitaxy precursors via RRKM theory. J Cryst Growth 106:227–238. https://doi.org/10.1016/0022-0248(90)90068-V

34. Mulvihill CR, Juárez R, Mathieu O, Petersen EL (2020) A Shock-Tube Study of the Rate Constant of PH3 + M ⇄ PH2 + H + M (M = Ar) Using PH3 Laser Absorption. J Phys Chem A 124:7380–7387. https://doi.org/10.1021/ACS.JPCA.0C04917

35. Ravi R, Takoudis CG (1992) Unimolecular Decomposition of Phosphine in Chemical Vapor Deposition Reactors. J Electrochem Soc 139:1994–2001. https://doi.org/10.1149/1.2069534

36. Semenov M, El-Kork N, Yurchenko SN, Tennyson J (2021) Rovibronic spectroscopy of PN from first principles. Phys Chem Chem Phys 23:22057–22066. https://doi.org/10.1039/d1cp02537f

37. Disanti MA, Fink U, Schultz AB (1990) Spatial distribution of H2O+ in comet P/Halley. Icarus 86:152–171. https://doi.org/10.1016/0019-1035(90)90205-N

38. Yumoto K, Saito T, Nakagawa T (1986) Hydromagnetic waves near O+ (OR H2O+) ion cyclotron frequency observed by Sakigake at the closest approach to comet Halley. Geophys Res Lett 13:825–828. https://doi.org/10.1029/GL013I008P00825

39. Bonev T, Jockers K (1994) H2O+ Ions in the Inner Plasma Tail of Comet Austin 1990 V. Icarus 107:335–357. https://doi.org/10.1006/ICAR.1994.1028

40. Wegmann R, Jockers K, Bonev T (1999) H2O + ions in comets: models and observations. Planet Space Sci 47:745–763. https://doi.org/10.1016/S0032-0633(98)00114-7

41. Consulting DCBS and, Antonio S, USA (2017) SUISEI—A Versatile Global Model of Comets with Applications to Small Solar System Bodies. J Appl Math Phys 05:311–320. https://doi.org/10.4236/JAMP.2017.52028

42. Barone V, Biczysko M, Bloino J (2014) Fully anharmonic IR and Raman spectra of medium-size molecular systems: Accuracy and interpretation. Phys. Chem. Chem. Phys. 16:1759–1787

43. Franke PR, Stanton JF, Douberly GE (2021) How to VPT2: Accurate and Intuitive Simulations of CH Stretching Infrared Spectra Using VPT2+K with Large Effective Hamiltonian Resonance Treatments. J Phys Chem A 125:1301–1324. https://doi.org/10.1021/acs.jpca.0c09526

44. Frisch MJ, Trucks GW, Schlegel HB, et al Gaussian 16 Revision B.01

45. Neese F (2012) The ORCA program system. Wiley Interdiscip Rev Comput Mol Sci 2:73–78

46. Weston RE, Nguyen TL, Stanton JF, Barker JR (2013) HO + CO reaction rates and H/D kinetic isotope effects: Master equation models with ab initio SCTST rate constants. J Phys Chem A 117:821–835. https://doi.org/10.1021/jp311928w

47. Nguyen TL, Barker JR (2010) Sums and densities of fully coupled anharmonic vibrational states: A comparison of three practical methods. J Phys Chem A 114:3718–3730. https://doi.org/10.1021/JP100132S/SUPPL_FILE/JP100132S_SI_001.PDF

48. Hernandez R, Miller WH (1993) Semiclassical transition state theory. A new perspective. Chem Phys Lett 214:129–136. https://doi.org/10.1016/0009-2614(93)90071-8

49. Miller WH (1974) Quantum mechanical transition state theory and a new semiclassical model for reaction rate constants. J Chem Phys 61:1823–1834. https://doi.org/10.1063/1.1682181

50. Brown NJ, Miller JA (1984) Collisional energy transfer in the low-pressure-limit unimolecular dissociation of HO 2. J Chem Phys 80:5568–5580. https://doi.org/10.1063/1.446621

51. Barker JR, Frenklach M, Golden DM (2015) When Rate Constants Are Not Enough. J Phys Chem A 119:7451–7461. https://doi.org/10.1021/acs.jpca.5b00640

52. Gilbert RG, Luther K, Troe J (1983) Theory of Thermal Unimolecular Reactions in the Fall-Off Range - 2. Weak Collision Rate Constants. Berichte der Bunsengesellschaft/Physical Chem Chem Phys 87:169–177. https://doi.org/10.1002/bbpc.19830870218

53. Dames EE, Golden DM (2013) Master equation modeling of the unimolecular decompositions of hydroxymethyl (CH2OH) and methoxy (CH3O) radicals to formaldehyde (CH2O) + H. J Phys Chem A 117:7686–7696. https://doi.org/10.1021/jp404836m

54. Robertson SH, Pilling MJ, Jitariu LC, Hillier IH (2007) Master equation methods for multiple well systems: application to the 1-,2-pentyl system. Phys Chem Chem Phys 9:4085–4097

55. Kuwata KT, Kujala BJ, Morrow ZW, Tonc E (2011) Quantum chemical and RRKM/master equation studies of cyclopropene ozonolysis. Comput Theor Chem 965:305–312. https://doi.org/10.1016/j.comptc.2010.10.019

56. Barker JR, Nguyen TL, Stanton JF, et al (2021) MultiWell-2021 Software Suite. In: J. R. Barker, Univ. Michigan, Ann Arbor, Michigan, USA. http://clasp-research.engin.umich.edu/multiwell/

57. Barker JR (2001) Multiple-well, multiple-path unimolecular reaction systems. I. MultiWell computer program suite. Int J Chem Kinet 33:232–245. https://doi.org/10.1002/kin.1017

58. Le XT, Mai TVT, Ratkiewicz A, Huynh LK (2015) Mechanism and kinetics of low-temperature oxidation of a biodiesel surrogate: Methyl propanoate radicals with oxygen molecule. J Phys Chem A 119:3689–3703. https://doi.org/10.1021/jp5128282

59. Carpenter BK (2013) Energy disposition in reactive intermediates. Chem Rev 113:7265–7286. https://doi.org/10.1021/cr300511u

60. Baptista L, Fernandes Francisco L, Dias JF, et al (2014) Theoretical study of Δ-3-(+)-carene oxidation. Phys Chem Chem Phys 16:19376–19385. https://doi.org/10.1039/c4cp02627f

61. Döntgen M, Leonhard K (2017) Discussion of the Separation of Chemical and Relaxational Kinetics of Chemically Activated Intermediates in Master Equation Simulations. J Phys Chem A 121:1563–1570. https://doi.org/10.1021/acs.jpca.6b12927

62. González-García N, Olzmann M (2010) Kinetics of the chemically activated HSO5 radical under atmospheric conditions – a master-equation study. Phys Chem Chem Phys 12:12290. https://doi.org/10.1039/c0cp00284d

63. Kumar PSV, Raghavendra V, Subramanian V (2016) Bader's Theory of Atoms in Molecules (AIM) and its Applications to Chemical Bonding. J Chem Sci 128:1527–1536. https://doi.org/10.1007/s12039-016-1172-3

64. Bader RFW (1991) A quantum theory of molecular structure and its applications. Chem Rev 91:893–928. https://doi.org/10.1021/cr00005a013

65. Bader RFW (1985) Atoms in molecules. Acc Chem Res 18:9–15. https://doi.org/10.1021/ar00109a003

66. Rubin M, Bekaert D V., Broadley MW, et al (2019) Volatile Species in Comet 67P/Churyumov-Gerasimenko: Investigating the Link from the ISM to the Terrestrial Planets. ACS Earth Sp Chem 3:1792–1811. https://doi.org/10.1021/acsearthspacechem.9b00096

67. Scattergood TW (1987) Laboratory experiments in the study of the chemistry of the outer planets. Adv Sp Res 7:99–108. https://doi.org/10.1016/0273-1177(87)90361-9

68. Nguyen T, Oba Y, Shimonishi T, et al (2020) An Experimental Study of Chemical Desorption for Phosphine in Interstellar Ice. Astrophys J Lett 898:L52.

https://doi.org/10.3847/2041-8213/aba695

69. Chantzos J, Rivilla VM, Vasyunin A, et al Astronomy The first steps of interstellar phosphorus chemistry. https://doi.org/10.1051/0004-6361/201936531

70. Zeng X, Beckers H, Willner H (2011) Elusive O=P≡N, a rare example of phosphorus σ 2λ 5-coordination. J Am Chem Soc 133:20696–20699. https://doi.org/10.1021/ja2091867

71. Grant DJ, Dixon DA, Kemeny AE, Francisco JS (2008) Structures and heats of formation of the neutral and ionic PNO, NOP, and NPO systems from electronic structure calculations. J Chem Phys 128:164305. https://doi.org/10.1063/1.2902983

72. Drozd GT, Kurtén T, Donahue NM, Lester MI (2017) Unimolecular Decay of the Dimethyl-Substituted Criegee Intermediate in Alkene Ozonolysis: Decay Time Scales and the Importance of Tunneling. J Phys Chem A 121:6036–6045. https://doi.org/10.1021/acs.jpca.7b05495

73. Omran A, Oze C, Jackson B, et al (2021) Phosphine Generation Pathways on Rocky Planets. Astrobiology 21:1264–1276. https://doi.org/10.1089/ast.2021.0034

74. Greaves JS, Richards AMS, Bains W, et al (2021) Phosphine gas in the cloud decks of Venus. Nat Astron 5:655–664. https://doi.org/10.1038/s41550-020-1174-4

75. Cardelino BH, Moore CE, Cardelino CA, et al (2003) Semiclassical calculation of reaction rate constants for homolytical dissociation reactions of interest in organometallic vapor-phase epitaxy (OMVPE). J Phys Chem A 107:3708–3718. https://doi.org/10.1021/jp026289j

76. Miller JA, Klippenstein SJ, Raffy C (2002) Solution of some one- and two-dimensional master equation models for thermal dissociation: The dissociation of methane in the low-pressure limit. J Phys Chem A 106:4904–4913. https://doi.org/10.1021/jp0144698

77. Stanton JF (2016) Semiclassical Transition-State Theory Based on Fourth-Order Vibrational Perturbation Theory: The Symmetrical Eckart Barrier. J Phys Chem Lett 7:2708–2713. https://doi.org/10.1021/ACS.JPCLETT.6B01239

78. Weston RE, Nguyen TL, Stanton JF, Barker JR (2013) HO + CO Reaction Rates and H/D Kinetic Isotope Effects: Master Equation Models with ab Initio SCTST Rate Constants. J Phys Chem A 117:821–835. https://doi.org/10.1021/jp311928w

79. Miller WH (1993) Beyond Transition-State Theory: A Rigorous Quantum Theory of Chemical Reaction Rates. Acc Chem Res 26:174–181. https://doi.org/10.1021/AR00028A007

80. Miller WH (2008) Semiclassical limit of quantum mechanical transition state theory for nonseparable systems. J Chem Phys 62:1899. https://doi.org/10.1063/1.430676

81. Brook RD, Rajagopalan S, Pope CA, et al (2010) Particulate matter air pollution and cardiovascular disease: An update to the scientific statement from the american heart association. Circulation 121:2331–2378. https://doi.org/10.1161/CIR.0b013e3181dbece1

82. Jasper AW, Miller JA (2011) Theoretical Unimolecular Kinetics for CH 4 + M ⇄ CH 3 + H + M in Eight Baths, M = He, Ne, Ar, Kr, H 2 , N 2 , CO, and CH 4. J Phys Chem A 115:6438–6455. https://doi.org/10.1021/jp200048n

83. Atkinson R, Arey J (2003) Atmospheric Degradation of Volatile Organic Compounds. Chem Rev 103:4605–4638. https://doi.org/10.1021/CR0206420

84. Larson HP, Fink U, Treffers RR (1977) Phosphine in Jupiter's atmosphere - The evidence from high-altitude observations at 5 micrometers. Astrophys J 211:972. https://doi.org/10.1086/155009

85. Kaye JA, Strobel DF (1984) Phosphine photochemistry in the atmosphere of Saturn. Icarus 59:314–335. https://doi.org/10.1016/0019-1035(84)90105-2

86. Fletcher LN, Orton GS, Teanby NA, Irwin PGJ (2009) Phosphine on Jupiter and Saturn from Cassini/CIRS. Icarus 202:543–564. https://doi.org/10.1016/J.ICARUS.2009.03.023

87. Irwin PGJ, Parrish P, Fouchet T, et al (2004) Retrievals of jovian tropospheric phosphine from Cassini/CIRS. Icarus 172:37–49. https://doi.org/10.1016/J.ICARUS.2003.09.027

88. Omran A, Oze C, Jackson B, et al (2021) Phosphine Generation Pathways on Rocky Planets. Astrobiology 21:1264–1276. https://doi.org/10.1089/ast.2021.0034

89. Lincowski AP, Meadows VS, Crisp D, et al (2021) Claimed Detection of PH 3 in the Clouds of Venus Is Consistent with Mesospheric SO 2. Astrophys J Lett 908:L44. https://doi.org/10.3847/2041-8213/abde47

90. Villanueva GL, Cordiner M, Irwin PGJ, et al (2021) No evidence of phosphine in the atmosphere of Venus from independent analyses. Nat Astron 5:631–635. https://doi.org/10.1038/s41550-021-01422-z

91. Milojevic T, Treiman AH, Limaye SS (2021) Phosphorus in the Clouds of Venus: Potential for Bioavailability. https://home.liebertpub.com/ast 21:1250–1263. https://doi.org/10.1089/AST.2020.2267

92. Zapata Trujillo JC, Syme A-M, Rowell KN, et al (2021) Computational Infrared Spectroscopy of 958 Phosphorus-Bearing Molecules. Front Astron Sp Sci 8:639068. https://doi.org/10.3389/fspas.2021.639068

93. Seager S, Bains W, Petkowski JJ (2016) Toward a List of Molecules as Potential Biosignature Gases for the Search for Life on Exoplanets and Applications to Terrestrial Biochemistry. Astrobiology 16:465–485. https://doi.org/10.1089/ast.2015.1404